Journal of
Materials Chemistry B

Materials for biology and medicine

Accepted Manuscript

This article can be cited before page numbers have been issued, to do this please use: L. E. Eccles, B. Foquet, A. Markee, R. K. Liwang, K. B. Basso, A. Y. Kawahara and W. L. Stoppel, *J. Mater. Chem. B*, 2025, DOI: 10.1039/D5TB01008J.

ROYAL SOCIETY OF CHEMISTRY

rsc.li/materials-b

View Article Online
DOI: 10.1039/D5TB01008J

Morphological and compositional basis of silk fiber function in *Actias luna*

Lauren E. Eccles,[1] Bert Foquet,[2] Amanda Markee,[2,3] Rebecca K. Liwang,[4] Kari B. Basso,[5] Akito Y. Kawahara,[2] Whitney L. Stoppel[1*]

[1]Department of Chemical Engineering, University of Florida, Gainesville, FL 32611, USA
[2]McGuire Center for Lepidoptera and Biodiversity, Florida Museum of Natural History, University of Florida, Gainesville, FL 32611, USA
[3]American Museum of Natural History, New York, NY 10024, USA
[4]Department of Biology, University of Florida, Gainesville, FL 32611, USA
[5]Department of Chemistry, University of Florida, Gainesville, Fl 32603, USA

*Correspondence:
Whitney L. Stoppel, PhD
1006 Center Drive
PO Box 116005
Gainesville, FL 32611
Whitney.stoppel@ufl.edu

Abstract:

Silk is a highly versatile natural protein fiber with a wide range of uses, yet its diversity in composition and function remains poorly understood across the tree-of-life. This study investigates the silk of the Luna moth, *Actias luna* (Saturniidae), known to produce high-density cocoons with distinct fiber characteristics. Despite the broad recognition of *A. luna* as an important species for research and education, its silk production, silk fiber composition, and properties remain under characterized, particularly in comparison to other Saturniidae and model species such as *Bombyx mori*. Building from the recently assembled *A. luna* genome, this study examines key repeat motifs and amino acid composition of the silk fibroin heavy chain (FibH) protein in relation to silk fiber properties across species. We assessed the physical properties of native and degummed *A. luna* silk fibers, evaluating the effects of degumming time and treatment on fiber morphology and mechanical properties. *Actias luna* silk fibers have similar properties to other saturniid silks, aligning with established trends that link fiber characteristics to structural protein composition. Silk gland architecture and regional composition shifts in *A. luna* were analyzed, highlighting differences that correlate to differential protein expression. Analyses of fiber characteristics were further expanded to silk fibers produced by *A. luna* at different developmental stages. Variation in larval characteristics, fiber morphology, and silk fiber composition across larval instars suggests that life stage-specific silk fiber function may stem from differences in protein expression and silk fiber use. These findings advance understandings of how evolutionary and developmental shifts influence silk fiber properties, providing a foundation for rational design of protein-based biomaterials with tunable mechanical and structural characteristics for biomedical applications.

Keywords: silk fibroin, crystallinity, Lepidoptera, Luna moth, Saturniidae

View Article Online
DOI: 10.1039/D5TB01008J

1. Introduction

Silk fibers are among the strongest and most versatile biomaterials on Earth and have played important economic and cultural roles throughout much of human history.[1] With nearly 160,000 described species, the order Lepidoptera represents one of the largest groups of silk-producing organisms. Lepidopteran larvae use silk in diverse ways including cocoon construction, protection from environmental factors and predators, water repellency, dispersion, and prey capture.[2-5] Lepidopteran silk fibers primarily consist of an inner structural core of silk fibroin proteins, surrounded by an outer functional coating containing sericins, seroins, and other supporting proteins.[5-7] The unmatched strength, stability, and extensibility of silk fibers is driven by the hierarchical structure of silk fibroin, derived from the highly repetitive and semicrystalline nature of fibroin proteins.[5, 6, 8, 9] The outer fiber coating, comprising approximately 30% of the native silk fiber, serves as a protective and adhesive layer that attaches to surfaces or other fibers.[5, 6, 9]

Recent advancements in long-read DNA sequencing technologies have significantly enhanced the ability to generate high quality lepidopteran genomes,[10, 11] leading to a surge in available genomes (e.g. Ag100 Pest Initiative,[12] Darwin Tree of Life[13]). More importantly, this sequencing revolution enables the comprehensive characterization of long, repetitive silk genes,[14] driving a sharp increase in both the number of identified silk genes and the species for which they are available.[15-18] Recent efforts focused on silk fiber genotype to phenotype relationships under varying environmental conditions[19, 20] or at different life stages[9, 21] have shown that fiber composition is dynamic, dependent on the needs of the insect. These changes in silk fiber composition can result in changes to fiber physical properties such as strength, elasticity, and hydrophobicity.[19, 22] With these advancements, the field is moving toward a deeper understanding of compositional differences and the roles that key proteins play in silk fiber structure, architecture, and function throughout an organism's life cycle across many silk-producing species.

The luna moth (*Actias luna*, Saturniidae), characterized by its tail-like hindwings and its bright green pigmentation (**Figure 1**), is common throughout the eastern United States and has one to three generations per year. The luna moth is popular as a model for research on insect chemical ecology and behavior[23, 24] and as an educational tool for children and the public.[25] *Actias luna* produces silk fibers throughout its lifetime, constructing strong silk cocoons for protection during pupation (**Figure 1Error! Reference source not found.**).[26, 27] Recently, a high-quality genome of *A. luna* was assembled, allowing for the characterization of silk genes and proteins, including fibroin heavy chain (FibH).[28, 29]

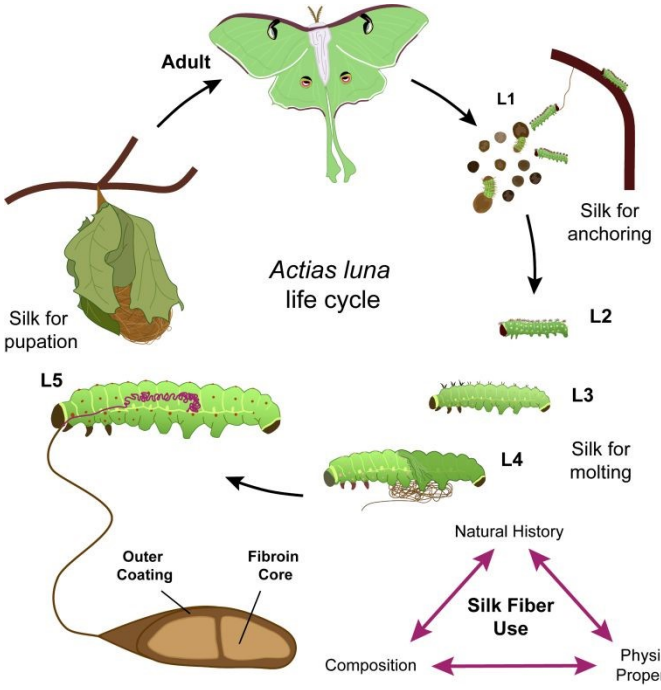

Figure 1: Life stages and silk fiber use in the Luna moth (*Actias luna*). Larvae produce silk throughout their life cycle and for different functions. L1: 1st instar, L2: 2nd instar, L3: 3rd instar, L4: 4th instar, L5: 5th instar.

Actias luna FibH possesses characteristic repeat motifs that form crystalline β-sheet

View Article Online
DOI: 10.1039/D5TB01008J

structures (polyA, $(GX)_n$) in silks across Saturniidae that correlate to their superior mechanical strength and stability.[5, 8, 28] Early characterizations of *A. luna* silk fibers have focused on its coarse, high-density cocoon and evaluated the ability to extract silk fibroin through degumming processes relevant to biomaterials research.[26, 27] Stemming from variations in amino acid composition, molecular weight, and overall repeat motif content and coverage in FibH proteins, wild silks produced by *A. luna* and many saturniid species offer alternatives to traditional silk-based biomaterials, such as films, sponges, and particles, derived from the mulberry silkworm, *Bombyx mori*.[30-33] Saturniid silk-derived biomaterials have primarily focused on *Antheraea* species (*Antheraea mylitta*, *Antheraea pernyi*) due to the presence of the tripeptide sequence RGD within their FibH protein, which promotes cell adhesion and tissue repair.[30, 31, 34] Other physiochemical and biological properties found in saturniid silks, such as differing amino acid composition, crystallinity (derived from different β-sheet repeat motifs, poly-alanine versus GAGAGS), and cocoon mineralization (calcium oxalate, zinc), could prove useful for many biomaterial applications.[8, 35, 36] However, the development of saturniid-derived biomaterials is limited often due to ease of laboratory rearing or silk collection, quality and amount of cocoon silk, and longer life cycles, relative to the cultivation of *B. mori*. *Actias luna* is easy to maintain under laboratory conditions and exhibits unique cocoon properties and fiber features that differ from that of model organisms like *B. mori*, *Antheraea yamamai*, and *Samia ricini*, despite being part of the same subfamily (Saturniinae) as the latter two species.[26, 36, 37] The extensive biodiversity of silk proteins produced by insects and spiders offers a large library of unique structural and functional proteins to study in the design and development of novel, naturally derived biomaterials.

In this study, we investigate the characteristics of silk gland structure, fiber composition and function, and material properties between *Actias luna* and closely related species. Whole organism micro-computed tomography (microCT) and histological analyses provide insight into the silk gland structure of *A. luna,* linking gland morphology and compositional shifts to silk fiber production. We build upon previous assessments of *A. luna* silk fibers by evaluating the physical properties of native and degummed fibers, focusing on morphological, structural, and mechanical stability differences upon removal of the outer fiber coating. The functional characteristics of *A. luna* silk fibers are driven, in part, by the composition and structure of silk fibroin heavy chain (FibH), supporting previously reported trends in the structure-function relationship in saturniid silk fibers.[5, 8] In addition to generating data on cocoon silk fibers, this work explores shifts in the morphology and function of fibers produced at different life stages. Larval growth and development are fundamentally dependent on silk fiber characteristics and production, utilizing silk fibers for molting and pupation, suggesting dynamic adaptations of fiber composition and function (**Figure 1**). These results present a detailed assessment of *A. luna* silk fiber and larval characteristics, furthering understandings into how the structure and composition of silk relate to physical properties.

2. Materials and Methods

2.1. *Actias luna* rearing

Actias luna caterpillars were reared in a US Department of Agriculture (USDA) containment lab at the University of Florida's McGuire Center for Lepidoptera and Biodiversity. All samples were collected from a single generation descended from wild-caught females in the southeastern United States, either in 2021 (computed tomography), 2024 (silk fiber properties and histology), or 2025 (larval growth measurements). Eggs were collected from gravid adult female moths and kept in large petri dishes until the eggs hatched.

View Article Online
DOI: 10.1039/D5TB01008J

Caterpillars that hatched within the same time period (2-3 days) were kept together in petri dishes or moved to clear plastic cups with lids. Caterpillars were fed fresh American sweetgum (*Liquidambar styraciflua*) and monitored every two days to keep track of their growth and the number of molting caterpillars, allowing accurate assessment of their larval stage. In 2021, caterpillars were reared to pupation in the clear cups and were moved to large flight cages containing American sweetgum branches upon pupation. In 2024 and 2025, they were transferred to a large flight cage after the third larval instar.

Actias luna growth and development was tracked by measuring head capsule size, larval length, and larval mass throughout the life cycle. Head capsule size was measured by placing larvae next to a ruler, imaging under a microscope, and then measuring the width of the head capsule in ImageJ analysis software.[38] Larval body mass was measured prior to molting to reduce fluctuations in mass as a function of feeding and growth during instar stage. Length was measured under a microscope, similar to head capsule size, as the larvae neared the end of their life stage, prior to molting.

2.2. FibH phylogenetic trees and repeat motifs

FibH protein sequences for *B. mori* and representative saturniid taxa were extracted from the NCBI database: *Bombyx mori* (NP_001106733.1), *Antheraea assamensis* (AIN40502.1), *Antheraea mylitta* (AAN28165), *Antheraea pernyi* (AAC32606.1), *Antheraea yamamai* (BAJ11925.1), *Actias selene* (ADA59934.1), *Samia ricini* (BAQ55621.1), *Hyalophora cecropia* (WWE94419), *Rhodinia fugax* (BAG84270), *Saturnia japonica* (BAH02016). To compare the terminal domains across phylogenetic groups, N-termini, C-termini, and concatenated N/C termini trees were created from FibH protein sequences. For each tree, the multiple sequence aligner MAFFT v7.490 in Geneious Prime® v2019.2.3 was used to align terminal sequences with a 1.53 gap penalty. With resulting alignments, phylogenetic trees were constructed using PhyML v.3.3.2 using default parameters with 1000 bootstrap iterations enabled. *Bombyx mori* was selected as an outgroup for all phylogenetic trees. *R. fugax*, *A. selene*, and *S. japonica* were excluded from C-termini and concatenated N/C termini alignments due to the lack of recovered C-termini in the reported partial sequence.

The *A. luna* FibH protein sequence was imported in Geneious Prime® v11.1.5 (https://www.geneious.com). FibH repeats were manually extracted and aligned using muscle v3.8.425.[39] The resulting alignment was used to generate a sequence logo,[40] showing the consensus sequence and relative amino acid frequency and information content (in bits) at every position in Geneious.

2.3. Computed Tomography (CT)

A fifth instar larva was fixed in 70% ethanol for two weeks prior to being submerged in a 1.25% Lugol's iodine contrast solution for seven days to allow visualization of soft tissues. The stained specimen was scanned on a GE Phoenix v|tome|x m 240 CT scanner with a 180 kV transmission tube and diamond target (General Electric, USA) at the UF Nanoscale Research Facility (Gainesville, Florida). Scan parameters were adjusted according to the specimen's size to produce a 21.79 µm voxel size at 80 kV voltage and 200 µA current. Generated 3D volume files were reconstructed with Datos|x CT software and processed with Volume Graphics VGStudio Max v2023.2. Silk glands were segmented with VGStudio segmentation tools and measured in VGStudio and ImageJ analysis software.[38]

View Article Online
DOI: 10.1039/D5TB01008J

2.4. Histological Sectioning and Staining

A fifth instar larva was fixed in phosphate buffered formalin (PBF) for 48 hours at 4°C (ThermoFisher Scientific, USA). To ensure full penetration of fixative throughout the insect, the outer skin layer was nicked by needle pins after 24 hours to improve diffusion into the larva. The fixed larva was then cut into sections and divided into individual cassettes before being returned to fixative overnight at 4°C. Fixed larval samples were dehydrated through a series of ethanol solutions before being transferred to xylene. Instar silk fibers were fixed in PBF before dehydration in ethanol and clearing in xylene. Dehydrated samples were placed in paraffin wax baths before embedding in paraffin blocks. Semi-thin sections (10 μm) were cut and mounted on glass slides. Larval sections were deparaffinized and rehydrated before being stained with hematoxylin and eosin (H&E) or DAPI and Phalloidin (ThermoFisher Scientific, USA). Silk fiber sections were deparaffinized and rehydrated before being stained with toluidine blue (ThermoFisher Scientific, USA). Stained sections were imaged on a Keyence BZ-X800 benchtop microscope.

2.5. Degumming

Cocoon (L5) silk fibers were degummed as described previously.[26] *Actias luna* cocoons were cut into pieces and boiled in a 0.5% (w/w) sodium carbonate and 10% (w/w) ethylenediamine solution for 30 minutes at a ratio of 2:1 silk mass (mg):volume of degumming solution (ml). Degummed silk fibers were rinsed in ultrapure water to remove residual salt (3 x 20 minutes) and air-dried for 48 hours. Mass loss upon degumming was determined by weighing the dried degummed mat relative to the initial mass of native cocoon fibers. To test the effect of degumming time on *A. luna* silk fibers, cocoon fibers were degummed for 15, 30, and 60 minutes (described in **Supplemental Figure S6**).

2.6. Proteomic analysis of *A. luna* silk glands

Expanded methods are described in **Supplemental Section 2**. Silk glands were dissected from fifth instar larva prior to spinning cocoons and snap frozen in liquid nitrogen. Samples were submerged in TRIzol and homogenized in a bead beater at 1900 rpm for 1.5 minutes. Samples were phase separated with chloroform and the organic protein-containing phase was retained. Proteins were precipitated from the organic phase by isopropanol precipitation according to manufacturer protocols. DNA was precipitated from the TRIzol lysate by adding 100% ethanol and incubating for 2–3 minutes before centrifuging at 2000 × g for 5 min at 4°C. The phenol–ethanol supernatant was transferred to a new tube, mixed with 1.5 mL of isopropanol per mL of TRIzol reagent, incubated for 10 min, and pelleted at 12,000 × g for 10 min at 4°C.

Proteins were extracted and digested using the EasyPep™ MS Sample Prep Kit (Thermo Fisher Scientific). Total protein was determined on a Qubit and the appropriate volume of each sample was taken to equal 20 μg total protein for digestion. Samples were digested with sequencing grade trypsin/lys C rapid digestion kit from Promega (Madison, WI) using manufacturer recommended protocol. MS analysis was immediately performed to ensure high quality tryptic peptides with minimal non-specific cleavage. Nano-liquid chromatography tandem mass spectrometry (Nano-LC/MS/MS) was performed on a ThermoScientific Q Exactive HF Orbitrap mass spectrometer equipped with an EASY Spray nanospray source (ThermoScientific) operated in positive ion mode and an UltiMate™ 3000 RSLCnano system (ThermoScientific).

All MS/MS spectra were analyzed using the Chimerys node (Thermo Fisher Scientific, San Jose, CA, USA; Proteome Discoverer 3.2.0.450). Chimerys was set up to search a custom curated fasta compiled from NCBI

View Article Online
DOI: 10.1039/D5TB01008J

GenBank[41] (accession numbers listed in **Supplemental Table S2,** downloaded 9/15/2025)[28, 29, 42-45] and Universal Protein Contaminants fasta[46] assuming the digestion enzyme trypsin. Chimerys was searched with a fragment ion mass tolerance of 0.020 Da and a precursor ion tolerance of 10.0 ppm. Carbamidomethyl of cysteine was specified in Chimerys as a fixed modification. Phosphorylation of serine, threonine, and tyrosine (STY) and oxidation of methionine was specified in Chimerys as a variable modification. Precursor ion intensity label free quantitation was done using Proteome Discoverer (Thermo Fisher Scientific vs 3.2.0.450). The two groups were compared using a "non-nested" study factor. Normalization was derived by using all peptides. Protein abundances were calculated by summed abundances, meaning the protein abundances are calculated by summing sample abundances of the connected peptide groups.

2.7. Scanning Electron Microscopy (SEM)

Silk was collected in each instar and kept at 4°C until analysis. At the first instar, silk was collected on branches and stems where multiple caterpillars had walked. In later instars, silk was exclusively collected from the silk pad, spun in preparation for their molt or from the cocoon. Silk fibers were secured to ZEISS/LEO SEM sample stubs with carbon conductive tape (Catalog No. 16202, Ted Pella, Inc., USA). L1-L4 fibers were sputter-coated with 8 nm of gold prior to imaging and analysis. Samples were dried overnight in air prior to imaging on a Phenom Pure benchtop SEM. Images were obtained using a backscattered electron detector with 5 kV acceleration voltage. Long axis fiber diameter measurements for each instar were completed in ImageJ analysis software[38] (n=90).

2.8. Fourier Transform Infrared (FTIR) Spectroscopy

Native and degummed cocoon silk fibers were analyzed using attenuated total reflectance (ATR) with a zinc selenide crystal on a Nicolet iS50 FTIR Spectrometer (ThermoFisher Scientific, USA) at the UF Nanoscale Research Facility (Gainesville, Florida). Sample spectra and background spectra were collected over 64 scans at a resolution of 4 cm^{-1} over a 4,000–650 cm^{-1} wavenumber range (n=6). Background spectra were subtracted from sample spectra in OMNIC™ Spectra Software and then analyzed with Origin data analysis software (OriginLab Corporation, USA). Deconvolution was performed within the amide I region (1590-1720 cm^{-1}) according to Hu *et al.*[47] to estimate protein secondary structure.

2.9. Thermal Gravimetric Analysis (TGA)

Native and degummed cocoon silk fibers were analyzed using TA Instruments TGA550 (TA Instruments, USA). Samples (5-10 mg) were placed in platinum pans (TA Instruments, USA, 957207.904) and ramped from ambient temperature to 500°C at 10°C/min with air flow of 40 L/min and N_2 flow of 60 L/min. Water content and T_d were determined using TA Instruments TRIOS analysis software.

2.10. Tensile Testing

Individual fibers were removed from cocoons or degummed silk mats and secured to thin paper frames. Frames were inserted into solid rectangular fixture (SRF) screw clamps of an Anton Paar MCT 702e Rheometer (Anton Paar, Graz, Austria). The gauge length of all samples prior to tensile testing was 10 mm. The sample in the paper frame was tightened to 10 centinewton/meter with a torsion screwdriver, and the side paper panels were cut with scissors once tightened. Anton Paar RheoCompass software was used to pre-stretch samples to 0.01 N and perform static extensional tests at 1 mm/min strain rate. Non-degummed

View Article Online
DOI: 10.1039/D5TB01008J

and degummed tensile tests were carried out under the same ambient temperature (25°C) and humidity (45-50%) conditions. Young's modulus (E), ultimate tensile strength (UTS), and strain at fracture (ε_{break}) were calculated from resulting stress-strain curves. Cross-sectional area for rheological assessment was determined using diameter and thickness measurements of silk fibers, based on SEM images.

2.11. Atomic Force Microscopy (AFM)

Individual silk fibers were secured to glass slides and scanned in air on a Nanowizard 4XP ZEISS LSM 900 AFM (Bruker, GER) in QI Advanced Imaging mode. Height images were performed with a RTESPA-300 cantilever (k = 40 N/m, f = 300 kHz) (Bruker, USA) calibrated on glass slides prior to scanning. Arithmetic average roughness (Ra) and root mean square roughness (Rq) of silk fiber surfaces were determined from the complete height histogram of a 1 μm x 1 μm scanned area (256 x 256 pixels) in JPK SPM Data Processing Software.

2.12. Statistical Analysis

Experimental data are primarily expressed as average ± standard deviation with a minimum n=3. GraphPad Prism 10.2.2 (GraphPad Software Inc., USA) was used for statistical analysis unless otherwise stated. Analysis was performed with appropriate-size analysis of variance (ANOVA) with Tukey's test post-hoc analysis. Statistical significance is reported as *p<0.05, **p<0.01, ***p<0.001, and ****p<0.0001 with key features shown in the figures and tables.

3. Results and Discussion

3.1. Sequence Diversity of FibH and structural implications in *A. luna*

Across Lepidoptera and Trichoptera, the fibroin heavy chain protein (FibH) is comprised of non-repetitive N- and C-terminal domains and a highly repetitive, structural core. The N- and C-terminal domains are largely conserved across Lepidoptera and species strains, believed to function in the secretion and assembly of silk proteins.[48] The repetitive region can vary largely within a species and across taxonomic families and orders, influencing the semi-crystalline structures present within silks and resulting fiber properties.[5, 8, 48, 49] To compare the terminal domains of *A. luna* FibH across phylogenetic groups, we created an N-terminal, C-terminal, and concatenated N/C terminal tree for heavy-chain fibroin (**Figure 2A**, **Supplemental Figure S1**). The non-repetitive amine terminal sequence (N-term) begins with a methionine amino acid residue and averages around 150 residues in model species (*B. mori*), inclusive of the signal peptide.[48, 49] Sequence alignment of 10 saturniid and *B. mori* N-terminal domains shows that terminal domains are highly conserved, with high alignment between genera (i.e., *Antheraea*, *Actias*) (**Figure 2A, Supplemental Figure S2**). The carboxyl terminal region (C-term) is found proceeding of the second largest exon and is far less conserved in sequence identity in lepidopterans. Thus, for C-terminal and concatenated NC terminal trees, we excluded sequences with partial C-term domains (**Supplemental Figure S1**).

Differences in the conserved termini domains of FibH proteins represent diverging evolutionary relationships based on spatial and temporal history (**Figure 2A**).[37] The diversity of structure and physical properties across silk fibers is more complex, emerging in part from sequence-level variations in the repetitive region in FibH proteins. Despite containing similar repetitive motifs (i.e., polyA, GX, GGX), the repetitive region exhibits interspecific and intraspecific variation in the length, order, and number of motifs, with the portion of amorphous and crystalline domains contributing largely to observed silk fiber properties.[5, 8, 48, 50-52] Similar to previous reports in a wide variety of silk-spinning taxa,[50, 51] *A. luna FibH*

View Article Online
DOI: 10.1039/D5TB01008J

exhibits allelic variation, even within one individual,[28] resulting in variation in its total length and repeat number.

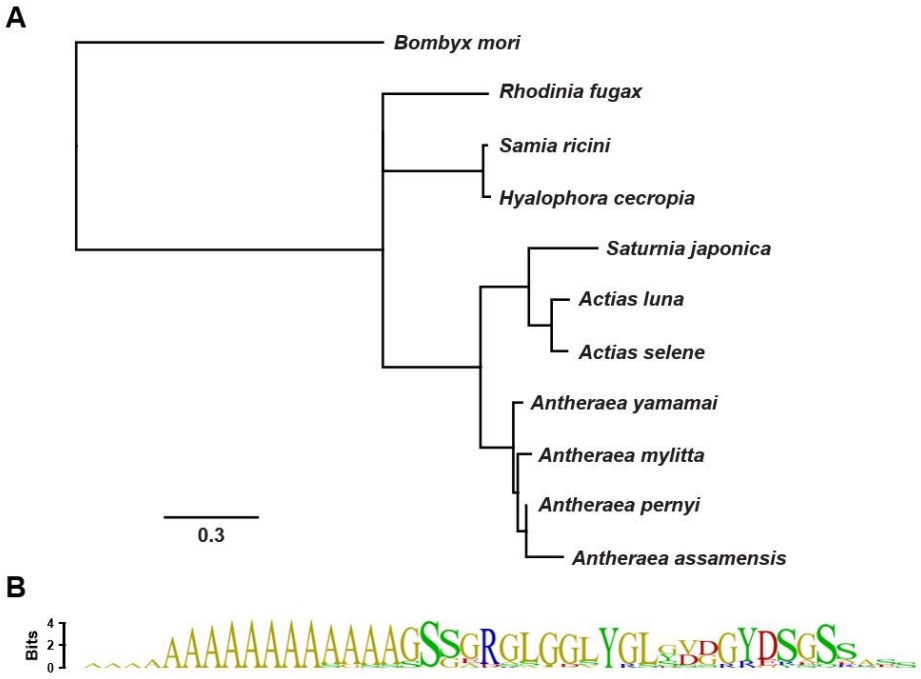

Figure 2. ***Actias luna*** **FibH structure and phylogeny.** (**A**) Phylogenetic tree generated by multiple sequence alignment of non-repetitive N-termini. Scale bar represents the number of amino acid substitutions per site, indicative of evolutionary change. (**B)** Sequence logo of the alignment of the 73 repeat sequences of *A. luna* FibH. Amino acids are colored based on their chemical nature (blue: basic, red: acidic, green: polar, yellow: non-polar). Larger font size is indicative of greater prevalence and conservation.

The primary *A. luna* FibH has a length of 2679 amino acids and contains 73 repeats, consisting of 21-77 amino acids with repeat motifs characteristic of other saturniid FibH proteins (**Figure 2B**).[8, 28, 45, 53-56] Each repeat in *A. luna* FibH begins with a stretch of 8-17 alanine residues (PolyA motifs, average length of 11 residues) followed by multiple glycine-rich motifs, GX and GGX (X is often Y, A, S, L).[5, 28] PolyA regions are hypothesized to form crystalline β-sheet structures, contributing to the rigidity and strength of saturniid silk fibers,[5, 8] in contrast to the hexapeptide GAGAGS in *B. mori* FibH that dominates its crystalline region.[57, 58] PolyA motifs are primarily observed in saturniid FibH among lepidopteran species, but their presence has recently been identified in the FibH of a few species of bagworms (Psychidae)[18, 59, 60] and is also common in multiple types of spidroin proteins.[61-63] Compared to other saturniid FibH proteins, *A. luna* FibH contains fewer GX and GGX motifs and a larger number of bulky, hydrophobic residues such as leucine (L) and valine (V) (6% and 2%, respectively, versus less than 1% in other species**Error! Reference source not found.**), which are correlated to silk strength and extensibility.[5, 8] The repeat motifs and amino acid composition of *A. luna* FibH reflect structural adaptations distinct from *B. mori* and shifted from other saturniids, potentially influencing the physical properties of *A. luna* silk fibers.

3.2. Structural and compositional characterization of *A. luna* silk glands

Morphological properties of silk glands relevant to expression, storage, and secretion of silk proteins are variable across silk-producing species, possibly due to differences in habitat, primary silk use, and timing of silk production.[64, 65] Silk glands are generally categorized into three distinct regions that differ in their

View Article Online
DOI: 10.1039/D5TB01008J

morphology, function, and secreted proteins.[66-71] The anterior silk gland (ASG) serves as an excretory duct, the middle silk gland (MSG) secretes sericins and other components of the outer coating, and the posterior silk gland (PSG) produces the contents of the silk fibroin core. Computed tomography (CT) presents a unique opportunity to visualize the complete structure of insect silk glands and other tissues without dissection, allowing the natural arrangement and structure of native tissues to be maintained.[72] Diffusible iodine-based contrast-enhanced CT was used to visualize the internal soft tissues of an *A. luna* fifth instar (L5) larva (**Figure 3**). Silk glands were segmented based on grayscale differences between tissues and visualized within the 3D reconstruction of the insect (**Figure 3A, Supplemental Video 1**).

3.2.1. Silk gland architecture in *Actias luna*

The paired silk glands of *A. luna*, corresponding to the two filaments in lepidopteran silk fibers, consist of curved, highly symmetric structures in the PSG and MSG and a thinner, more linear morphology in the ASG (**Figure 3B**). Each gland of the fifth instar *A. luna* larva is approximately 80 mm when measured end-to-end and occupies a volume close to 3 mm^3. Relative to the insect, the linear silk gland length is double the length of the larva (40 mm) and occupies about 0.18% of the total volume of the larva (1590 mm^3). Measurements of silk gland diameter throughout the full length of segmented silk glands (**Figure 3CD**) show consistency in dimensions between the two glands; however, morphological boundaries between the MSG and PSG were unable to be clearly visualized. Tapering of silk gland diameter is observed towards the ASG and spinneret (200 to 90 µm), while the diameter within the MSG and PSG is more variable, between ~150 and 340 µm.

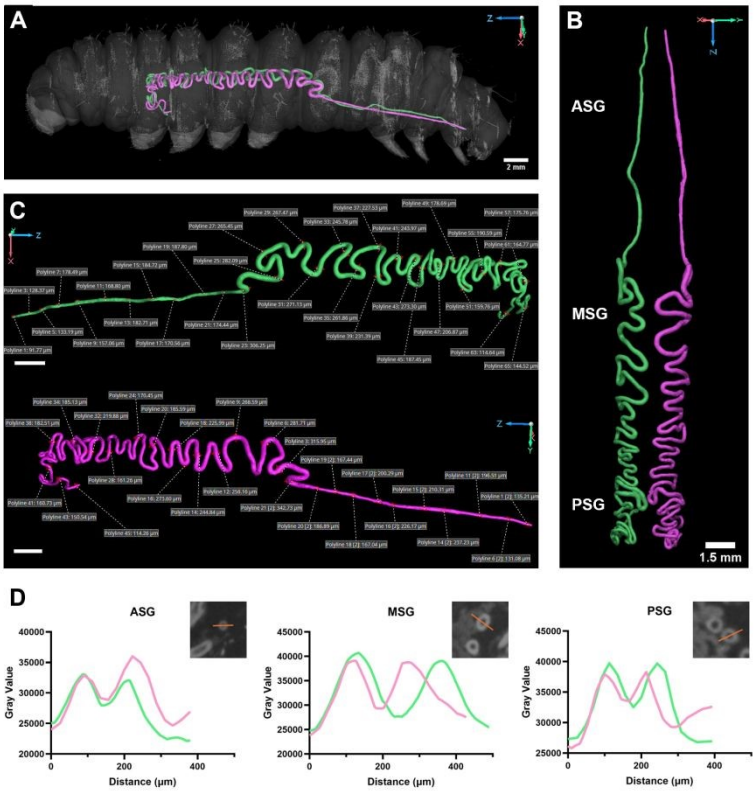

Figure 3. ***Actias luna*** **silk gland structure** ***in situ*****.** (**A**) 3D reconstruction of a L5 larva, viewed laterally, depicting silk glands segmented in pink and green. (**B**) Dorsal view of segmented silk glands oriented with the larva's head at the top of the image. (**C**) Measurements throughout silk gland length. Scale bars are 1.5 mm. (**D**) Representative grayscale line profiles through the cross section of *A. luna* silk glands in the ASG, MSG, and PSG. Green and pink lines correspond to the similar colored glands in (A-C).

Observed silk gland morphology is similar to those reported for other Saturniidae, and distinctly different from the silk glands of the domesticated silkworm, *B. mori*.[42, 56, 64, 73, 74] The appearance of long, thinner glands in Saturniidae is hypothesized to correlate to lower resource allocation to silk production and overall smaller amounts of silk produced.[64] This is primarily driven by the lack of clear storage structures and the structural similarities between the MSG and PSG (**Figure 3B** and **C**, **Figure 4**), which is unlike *B. mori* silk glands that possess large, swollen MSGs essential to longer storage times and high levels of silk production for cocoon construction.[6, 64] Although comparative volumetric

View Article Online
DOI: 10.1039/D5TB01008J

assessments are not commonly reported in literature, the low silk gland volume with respect to total insect volume (0.18%) could prove analogous to wet mass ratios reported by Holland *et al.*[64] Larger percent mass ratios of silk gland dope to total insect mass correlated to insects with high silk production, while lower mass ratios, specifically reported for *A. selene* and *A. yamamai*, were suggested to correlate to lower resource allocation for silk production and low storage time of silk dope in the gland.[64] *Actias luna* produces thin, loosely packed, single-layer cocoons,[26, 27] aligning with the hypothesized link between silk gland structure and overall silk production.[64] Continued efforts toward a more in-depth comparison of silk gland structures is required to better elucidate the relationship between silk gland structure and silk production.

3.2.2. Regional variation in silk gland composition

The *A. luna* silk gland exhibits morphological and compositional variation throughout relative gland regions (**Figure 4**). Narrow, thin ASG cross sections (**Figure 4A**) are easily distinguished from the thicker medial and posterior gland regions (**Figure 4B** and **C**, respectively). Slight variation between silk gland size observed between insects used for CT and histological studies could result from differences within the specimen prep for analysis and potential differences in the stage of insect (close to pupation vs. early instar). Although we were unable to determine the specific boundaries between the MSG and PSG regions based on morphology alone, compositional differences within silk gland cross sections indicate changes in the expression and composition of proteins within cell secretions. The appearance of a two-phase organization is visualized within gland cross-sections of the MSG (**Figure 4B**) while the PSG has a primarily homogenous cross-section (**Figure 4C**), indicating minimal compositional differences. Similar differences in transverse gland sections in the MSG and PSG were observed in related saturniid species, *H. cecropia* and *A. yamamai*.[42, 43] Identification and annotation of *A. luna* silk proteins is limited relative to other species. However, analysis of FibH and, more recently, eight putative sericin proteins,[29] suggests that the silk glands of *A. luna* are responsible for the production of similar proteins to other saturniid silkworms. Additionally, similarities in gland morphology and observed cocoon morphology and properties support the hypothesis that protein production and spinning behavior in *A. luna* follows that of closely related species. Thus, the two-phase structure within the MSG can be attributed to the presence of both silk coating proteins (sericins, seroins), expressed within the MSG, and silk fibroin, expressed in the PSG. Polyploid cells responsible for the production and secretion of silk proteins are visualized in both the MSG and PSG (**Figure 4DE**).

View Article Online
DOI: 10.1039/D5TB01008J

To expand on analyses of silk gland composition and identified *A. luna* silk proteins, silk glands from L5 larva prior to cocoon construction were dissected and pooled for proteomic analysis (3 biological replicates). We utilized two libraries as a foundational reference for identifying proteins: (1) an expanded

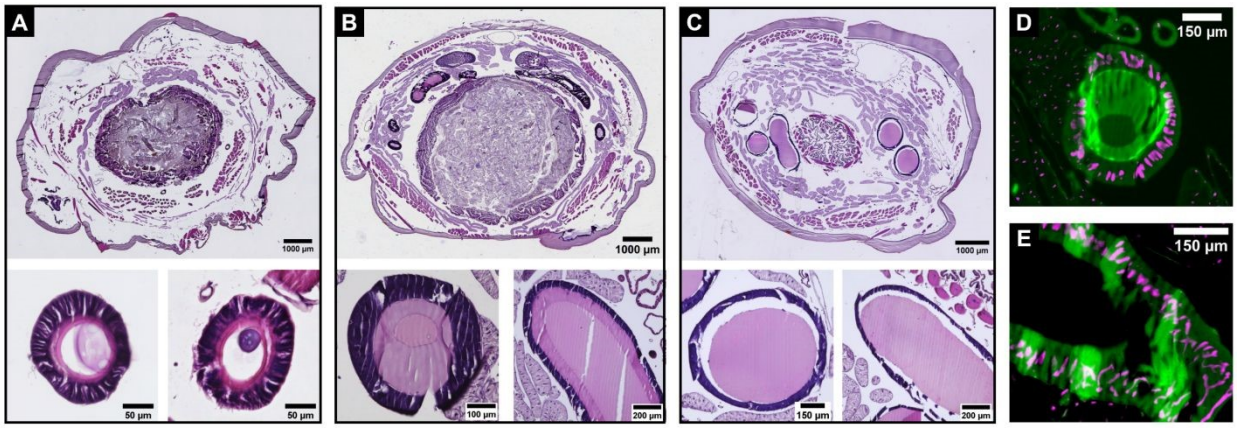

Figure 4. Histology of *A. luna* silk glands. Histological cross-sections of *A. luna* larva stained with hematoxylin and eosin in the (**A**) ASG, (**B**) MSG, and (**C**) PSG (dorsal side at the top of each image). Inset images show silk glands at higher magnification to visualize protein secretions within the lumen. Histological section of (**D**) MSG and (**E**) PSG stained with DAPI (nuclei, pink) and Phalloidin (f-actin, green), showing polyploidy.

library that includes *A. luna* proteins, silk-specific proteins identified for other saturniids, and proteins annotated from *B. mori* genome and (2) a restricted library limited to identified *A. luna* proteins, many of which were recently identified through genomic and transcriptomic analyses[28, 29] (accession numbers listed in **Supplemental Table S2**). This assessment of *A. luna* silk gland composition is preliminary and limited, both due to the number of identified proteins in *A. luna* and the lack of available functional genome annotations for saturniid species available through UniProt or the Protein Database available from the National Library of Medicine's National Center for Biotechnology Information (NCBI). Thus, the identification and comparisons of identified proteins are based on relative abundance compared to total abundances (**Supplemental Files 1, 2**) and not quantitatively assessed.

Through utilization of the expanded library, over 500 proteins were identified that play roles in protein metabolism (*e.g.,* proteases, dehydrogenases, juvenile hormone), cell organization (*e.g.,* cytoskeletal, transport), and stress response (*e.g.,* heat shock proteins, antioxidant enzymes). Identified *A. luna* silk proteins through this library were limited to FibH, Sericin A, and Sericin C, comprising approximately 3% of the total protein composition based on reported abundances (**Supplemental File 1**). In our recent collaborative work,[29] Sericin A and Sericin C were identified through sequence homology to other saturniid sericins and shared sericin protein motifs and termini (Ser A contig: ptg000025l; SerC contig: ptg0000811). Sericin A and C have been reported to share similar expression patterns (higher expression levels in later instars, primarily L4), though some variability across the population was noted.[29] In addition to shared expression patterns, the similar predicted amino acid composition suggests these sericins may serve a similar purpose within silk fiber structure. These proteomic analyses represent the first attempt to confirm the presence of proteins identified through genomic and transcriptomic assessments, specifically aimed at identifying these proteins in late-stage silk glands. Common reference genes for normalizing gene expression such as β-tubulin and actin were also identified, with consistent abundances across each sample (1.1 ± 0.03% and 0.61 ± 0.2%, respectively). Comparing silk gland proteomic data to the restricted library of *A. luna* putative proteins resulted in the identification of FibH and Sericin C in all three samples at a

View Article Online
DOI: 10.1039/D5TB01008J

relative expression ratio of 1:4. Sericin E was identified in one sample and at low abundance (<1%) (**Supplemental File 2**). Though limited, this assessment confirms the presence of a few putative sericin genes identified in *A. luna*[29] and relative expression patterns that suggest that, to an extent, differential gene expression patterns translate to observed protein composition within the silk glands. Further analyses are warranted to supplement this assessment and similar studies, both in *A. luna* and other saturniid species, to better elucidate links between the genetic blueprint, functional proteins, and overall biological function.

3.3. Impact of degumming on the structure and properties of *A. luna* silk fibers

3.3.1. Morphological and structural organization of *A. luna* silk

Actias luna silk fibers were degummed to evaluate sericin removal and silk fibroin-specific shifts in physical properties. SEM of native cocoon fibers (**Figure 5A**) reveal a tightly packed, yet slightly porous, network of interweaving, double-stranded fibers connected by an outer sericin-rich coating. *Actias luna* silk fibers appear ribbon-like, exhibiting an average long-axis fiber diameter of 41.9 ± 3.4 μm and flattened cross-sections (**Figure 5AB**), similar to previous reports.[26, 27] Degumming *A. luna* fibers for 15, 30, and 60 minutes resulted in the separation of the two fibroin filaments (average fiber diameter 18-20 μm) and revealed internal fibrillar structures aligned along the fiber axis (**Figure 5AB**, **Supplemental Figure S6**). Fibers degummed for 15 minutes exhibited an 18-20% mass loss while both 30- and 60-minute degummed silk had a mass loss between 25-35%. This suggests that 30 minutes of degumming is sufficient to remove the hydrophilic, sericin-rich coating and surface debris (**Figure 5B**) and that silk fibroin comprises around 70% of native *A. luna* silk fibers. Small crystal structures observed on the surface of native (non-degummed) *A. luna* fibers were visibly removed at longer degumming times (**Figure 5A**). As previously reported across Saturniidae,[8, 26, 27, 31, 42, 43, 75, 76] these crystals indicate the presence of calcium oxalate, which is secreted during cocoon construction and hypothesized to aid in the insulation and protection of cocoons.[27, 77] The presence of calcium oxalate on non-degummed fibers and removal of calcium oxalate upon degumming

View Article Online
DOI: 10.1039/D5TB01008J

was confirmed the presence and loss of the 1315 cm^{-1} peak at in FTIR spectra (**Supplemental Figure S7**), characteristic of calcium oxalate hydrate.[27, 75, 76]

FTIR analysis was also used to estimate protein secondary structures within fibers through deconvolution of the amide I peak (1700-1600 cm^{-1}, **Figure 5C**). Non-degummed and degummed *A. luna* silk fibers are both semicrystalline, with almost half of their secondary structure composed of β-sheets (46 ± 6% and 50 ± 2%, respectively). These crystalline β-sheet structures are largely attributed to the poly-alanine sheets (characteristic peak at 965 cm^{-1})[75, 76] and glycine rich GX motifs (X is often S, L, Y, A) present within the *A. luna* FibH (**Figure 2B**). Degumming *A. luna* silk fibers did not significantly shift the relative content of protein secondary structures determined within the silk fibers. The contributions of sericins and other

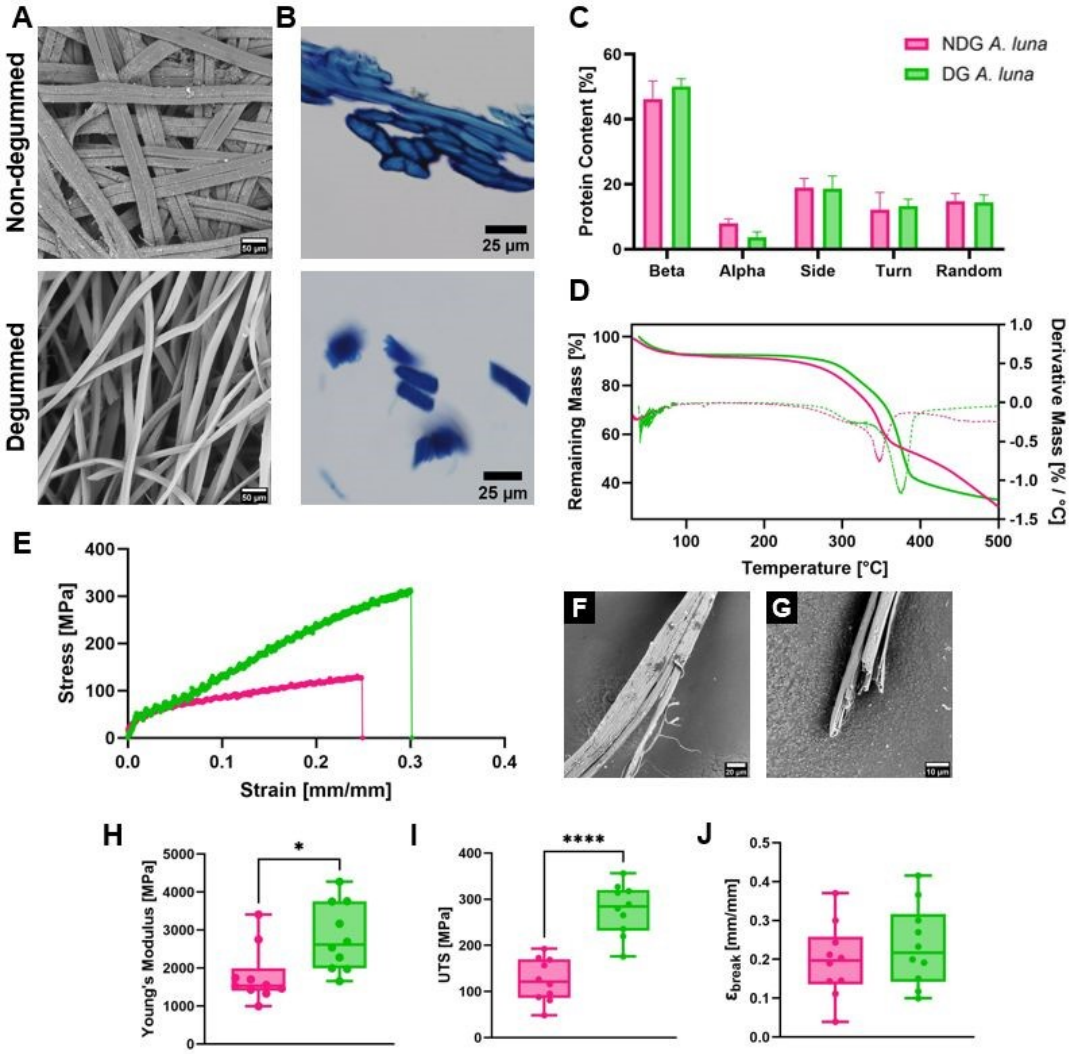

Figure 5. Degumming impacts on *A. luna* silk fiber structure and composition. (**A**) SEM image of non-degummed and degummed cocoon silk fibers. (**B**) Histological cross-section of non-degummed and degummed fibers stained with toluidine blue. The inner core of the fiber is a lighter blue than the outer coating. (**C**) Relative protein content determined through deconvolution of the amide I peak of FTIR spectra. Data is expressed as mean ± standard deviation (n=3). (**D**) Representative mass loss (solid line, left y-axis) and derivative mass loss curves (dashed line, right y-axis) of non-degummed (NDG, pink) and degummed (DG, green) *A. luna* silk determined through TGA. (**E**) Representative stress-strain curves of non-degummed and degummed fibers obtained from static tensile tests at 1 mm/min. Representative SEM images of fractured (**F**) non-degummed and (**G**) degummed fibers after tensile tests. (**H**) Young's modulus, (**I**) ultimate tensile strength, and (**J**) strain at break were determined from stress-strain curves (n=10). Analyzed with unpaired parametric t-test. Statistical significance is reported as *p<0.05 and ****p<0.0001.

View Article Online
DOI: 10.1039/D5TB01008J

coating proteins to silk fiber secondary structures and function in *A. luna* and other species are not yet fully understood, as the structure and interactions between proteins are highly complex and species dependent. However, the organization and interactions of *A. luna* silk fibroin are hypothesized to be modified through the removal of these proteins and exposure to harsh conditions during degumming, resulting in distinct physical properties from native silk fibers.

3.3.2. Effects of degumming on silk fiber stability and tensile properties

The balance between flexible and crystalline structural regions is thought to play an important role in determining the physical properties of silk fibers, particularly their thermal and mechanical characteristics. Degumming has been previously reported to directly influence the mechanical and thermal properties of silk fibers,[78, 79] both through removal of sericins and exposure of silk fibroin to high heat and chemical treatments. TGA analysis was used to evaluate the thermal stability of *A. luna* silk (**Figure 5D**). Non-degummed and degummed cocoon fibers exhibited an initial mass loss (7-9%) around 100°C upon evaporation of surface bound water. Further heating led to fiber degradation, beginning at around 280°C for non-degummed and 300°C for degummed silk fibers. Decomposition of non-degummed and degummed fibers occurs in the range of 350-400°C. The midpoint degradation temperature upon degumming was significantly shifted from 346°C (non-degummed) to 376 °C (degummed, $p=0.007$). Degradation of *A. luna* silk fibers occurs at lower temperatures than values reported for other saturniid silks that range between 360-380°C.[8, 31] The lower polyA content of *A. luna* FibH (34%) compared to other saturniid silks evaluated previously (39-43%) aligns with trends noted in prior literature, wherein increasing polyA correlates to a higher thermal stability (**Supplemental Figure S8**).[5, 8]

Tensile tests were performed to determine the Young's modulus (E), ultimate tensile strength (UTS), and strain at fracture (ε_{break}, extensibility) of individual non-degummed and degummed cocoon silk fibers. Representative stress-strain curves are shown in **Figure 5E**. *Actias luna* silk fibers exhibit an initial elastic region at low strain, followed by a strain-stiffening response, ultimately leading to a break or fracture at maximum stress. Non-degummed fibers often frayed or split upon extension (**Figure 5F**), while degummed fibers had a more brittle fracture across the fiber cross section (**Figure 5G**). Non-degummed silk fibers exhibited a significantly lower Young's modulus ($p=0.0120$) and ultimate tensile strength ($p<0.0001$) than degummed silk fibers (**Figure 5HI**). Degumming processes remove the sericin-rich coating that binds together silk fibroin filaments and modify the protein structures present within silk fibers (i.e., amorphous and crystalline structures, molecular weight, hydrophilic content),[80] influencing the response to stress or tensile loading. Although the effects of degumming are not fully understood, degumming *A. luna* fibers led to an increase in Young's modulus (NDG: 1790 ± 690 MPa, DG: 2801 ± 843 MPa) and ultimate tensile strength (NDG: 125 ± 45 MPa, DG: 278 ± 52 MPa). The strain at break, or extensibility, of *A. luna* silk fibers was highly variable and not significantly shifted between non-degummed (0.2 ± 0.09) and degummed (0.23 ± 0.10) fibers (**Figure 5J**).

View Article Online
DOI: 10.1039/D5TB01008J

The stress-strain profile and determined mechanical properties of non-degummed and degummed *A. luna* silk fibers are similar to other saturniid silks reported previously.[8] Despite variations in mechanical assessments, the mechanical properties of *A. luna* cocoon silk are of a similar magnitude to other saturniid silks and align with trends observed across the eight saturniid species examined by Malay *et al.*[8] Compositional differences in FibH proteins, such as the higher proportion of bulky hydrophobic residues (L,V) and a decreased abundance of elastic GGX motifs within the repetitive region of *A. luna* FibH (**Figure 2B**), could contribute to the lower extensibility and the brittle response of *A. luna* fibers compared to *Antheraea* silk (**Supplemental Figure S8**), as hypothesized for another species of *Actias*.[8] It is also important to note the differences in strain rate of tensile tests between the study by Malay *et al.* (10 mm/min),[8] Reddy *et al.* (18 mm/min),[26] and this study (1 mm/min). Differences in strain rate can skew mechanical property comparisons, as the viscoelastic properties of silks suggests strain-rate dependence.[78, 81] As the dynamics of silk protein sequence-structure-function relationships are highly complex interactions to explore, clear correlations are not observed in many physical properties (i.e., tensile modulus, toughness, strength).[5, 8, 61] This suggests that while FibH is thought to be the primary driver of physical properties, other protein constituents of silk fibers (sericins, seroins) or the interactions between fibroins and coating proteins also play an important role in fiber function.

3.4. Life stage-specific changes in *Actias luna* silk fibers

A substantial number of silk fiber studies focus on comparative analyses at a single life stage – often the final instar before pupation or the cocoon itself – to investigate genotype to phenotype relationships within and between species. Variations in fiber characteristics across life stages remain largely unexplored, primarily due to the lower silk volume produced in early instars, the ease of cocoon silk collection in both laboratory culture and field settings, and the lack of comparable studies in literature. Larval and silk fiber characteristics vary as *A. luna* larva progress through developmental stages, with the largest change observed between the fourth and fifth instar. The growth and development of *A. luna* larva was assessed throughout their life cycle by measurement of insect head capsule, length, and mass prior to molting (**Table 1**, **Supplemental Figure S9**). The head capsule size remains constant within a single developmental stage, and as larvae develop into the next instar, the old head capsule will be shed during the molting process and is replaced by a new, larger capsule. Head capsule size increased in each stage by an average factor of 1.5

Table 1. Life cycle characteristics of the Luna moth. Larval and silk fiber property values are reported as the average ± standard deviation (n ≥ 6).

Instar	*Head capsule width [mm]*	*Larval Mass [mg]*	*Larval Length [mm]*	*Fiber Diameter [μm]*	*Fiber Roughness [nm]*
L1	1.00 ± 0.05	19.50 ± 1.05	8.78 ± 0.56	3.1 ± 0.5	Ra: 8.5 ± 5.2 Rq: 10.4 ± 6.1
L2	1.55 ± 0.08	63.50 ± 6.02	11.06 ± 0.98	3.9 ± 0.7	Ra: 10.0 ± 4.2 Rq: 13.5 ± 4.7
L3	2.34 ± 0.09	295.89 ± 21.65	17.51 ± 2.06	7.1 ± 1.2	Ra: 11.3 ± 6.1 Rq: 14.3 ± 7.5
L4	3.38 ± 0.07	1519.74 ± 156.40	25.75 ± 1.67	11.2 ± 2.0	Ra: 11.1 ± 2.9 Rq: 13.3 ± 3.1
L5	5.09 ± 0.16	4615.75 ± 686.35	48.58 ± 5.36	41.9 ± 3.4	Ra: 13.8 ± 2.9 Rq: 17.2 ± 3.8

View Article Online
DOI: 10.1039/D5TB01008J

(Dyar's ratio),[82] while larval length and mass increased almost exponentially (**Table 1**, **Supplemental Figure S9**). The life cycle of *A. luna* and other silkworms are strongly associated with the production and use of silk fibers, ensuring that fiber output meets on the specific needs of the insect.

In *A. luna*, caterpillars begin producing silk immediately after emerging from their eggs (L1), using it as a safety line to anchor themselves to their host plant, allowing them to drop but remain suspended from the plant when encountering danger (**Figure 1**). In later instars (L2-L4), silk production decreases and primarily serves as a silk mat for molting (**Figure 1**). These silk mats, commonly found across Lepidoptera, serve as an important attachment point for shedding exuviae, significantly improving the ease and success of each molt (**Supplemental Figure S9**). Silk production is negligible in final instar caterpillars (L5) when caterpillars are actively feeding. Once caterpillars reach their maximum body size and an optimal pupation site is found, they significantly increase silk production to generate a single-layered, light brown cocoon wrapped in leaves (**Figure 1**).[26, 27] Like most cocoons, its main function is to protect and insulate the pupa during metamorphosis. The different silk uses in *A. luna* (safety line, silk mat, and cocoon) likely differ in properties, possibly stemming from differential expression of silk proteins and motivating efforts to identify these proteins in *A. luna*.

Throughout their development, *A. luna* silk maintains a double-stranded fiber morphology (**Figure 6A**) with fiber diameter increasing as the insect grows (**Table 1**, **Supplemental Figure S9**). The greatest increase in long-axis fiber diameter occurs between the 4th and 5th instar, as cocoon silk fibers are more than twice the diameter of fibers produced in L4. AFM analysis of fiber surface topography revealed differences in nano-scale features across larval instars (**Figure 6BC**). Various globular structures were observed on the silk surface, mostly unaligned or randomly oriented with respect to the fiber axis. These structures vary in morphology and size, contributing to slight differences in calculated surface roughness (**Table 1**). However, clear trends between arithmetic average roughness (Ra) and root mean square roughness (Rq) of instar silks were difficult to ascertain as no statistical significance between stages was found (**Supplemental Table S3**). Variations in surface features could indicate changes in silk fiber functional characteristics that are dependent on many factors within the insect's growth and development, such as fiber use (molting mat, cocoon), scale of silk production, spinning speed, or protein composition.

Larval silk fiber characteristics are influenced by both the structural core, consisting largely of silk fibroin, and the outer functional coating on the fiber, consisting largely of sericins and other supplemental proteins (**Figure 6D**).[5, 6, 83] Histological cross-sections of fibers produced during the second to fifth instar stained with toluidine blue indicate compositional differences in fibers produced at different life stages (**Figure 6E**). The intensity of the blue staining in the inner fibroin core remains constant throughout the development of *A. luna*, suggesting minimal compositional differences within the structural core of the silk fibers. This is consistent with the presence of a single fibroin protein in *A. luna* (**Figure 2**), previous reports of *B. mori* instar silks, and recent gene expression data by Foquet *et al*.[9, 28, 29] However, variation in staining intensity was observed in the outer coating between instars (**Figure 6D**), suggesting differences in the protein composition of the outer coating as a function of life stage. Specifically, in fifth instar cocoon fibers, the outer coating is a dark and purplish blue, contrasting with the coating of early instar (L2-L4) fibers, which are light blue to transparent. As the outer coating of lepidopteran silk fibers is primarily composed of sericins,[7, 42, 84] variation in staining across different life stages could be largely influenced by shifts in the expression and proportions of sericin proteins. Life stage-specific expression of *A. luna* silk proteins is supported by findings across Lepidoptera, with differences in expression directly linked to variations in silk characteristics.[9, 69] Identified *A. luna* sericins have variable amino acid composition, characteristic repeats,

View Article Online
DOI: 10.1039/D5TB01008J

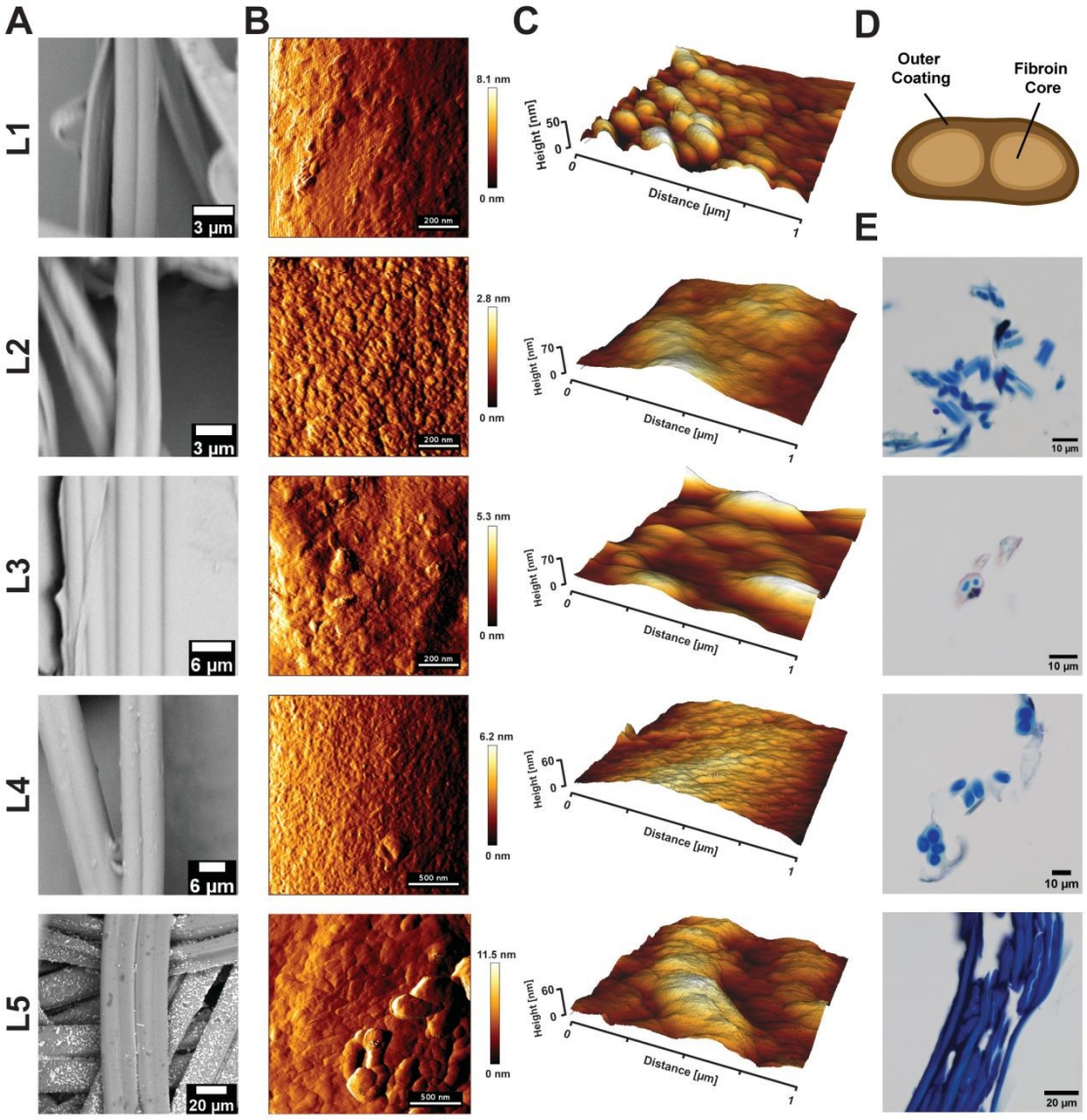

Figure 6. Imaging and characterization of *A. luna* silk fibers at each life stage. (**A**) Representative SEM images of silk fibers produced by each larval stage. (**B**) Two-dimensional and (**C**) three-dimensional height topographical AFM images of silk fibers produced at each life stage. Distributions of height scale in AFM images are depicted by the color scale (B) or height axis (C) accompanying the image. (**D**) Schematic representation of *A. luna* fiber cross section showing the inner fibroin core surrounded by the outer sericin-rich coating. (**E**) Histological cross-sections of L2, L3, L4, and L5 instar silk fibers stained with toluidine blue.

and expression profiles in early and late stage larva, suggesting these proteins play specific roles in the formation of silk fibers and life stage-specific silk use.[29] These compositional differences could also contribute to the observed differences in visual surface topography and roughness on the outer surface of silk fibers (**Figure 6BC**), modifying how the fibers would adhere to surfaces and other fibers or respond to environmental conditions at each life stage.

View Article Online
DOI: 10.1039/D5TB01008J

4. Conclusions

Actias luna produces silk throughout its life cycle, yielding fibers with distinct structural and functional characteristics at each stage. This study provides a broad investigation of *A. luna* silk, and its underlying structural and compositional bases. An analysis of silk gland morphology reveals shared traits among Saturniidae, which correlate with the capacity for silk fiber production and storage. Through comparative analyses, this study highlights the conservation of terminal regions and divergence of amino acid repeats of FibH protein within Saturniidae, contributing to the rapid evolution of silk proteins and the composition of *A. luna* silk fibers. Properties of native and degummed *A. luna* cocoon silk fibers – specifically the structural, thermal, and mechanical properties – are comparable to silks of other saturniid species, aligning with trends observed in the prediction of physical properties based on FibH protein sequences. Moreover, the morphological and compositional characterization of silk produced throughout the *A. luna* life cycle provides valuable insights into developmentally regulated shifts in silk fiber properties.

These results contribute to a broader understanding of protein evolution and functional diversification of lepidopteran silk fibers, underscoring the importance of combining multiple approaches to better understand silk fiber structure in relation to species and life stage. Our data furthers hypotheses that silk fiber properties are primarily driven by the structural protein FibH but also suggests that differences in properties and the utility to the insect could stem from variation in other proteins that comprise silk fibers (coating proteins) and overall silk production. These variations were observed at a single life stage between several saturniid species (cocoon silks), but also at multiple life stages within *A. luna* silk fibers. These results provide greater insight into structure-function relationships and key amino acid motifs as we move toward material applications or rational design of silk-like protein fibers.

5. Data Availability

The data supporting this article can be accessed here and is included as part of the supporting information. Supplementary information: FibH sequence alignment, degummed silk fiber imaging, FTIR spectra, physical property correlations, insect and fiber growth characteristics across life stages.

6. Acknowledgements and Funding

This work was conducted in part at the Research Service Centers of the Herbert Wertheim College of Engineering at the University of Florida with the valuable assistance of Dr. Edward Stanley and Dr. Gary Scheiffele. Proteomic data was obtained through the Mass Spectrometry Research and Education Center at the University of Florida in collaboration with Dr. Kari Basso (NIH S10 OD021758-01A1 and NIH S10 OD030250-01A1). We thank Paul Frandsen, Paul Masonick, and Bryce Shirk for providing valuable feedback on the manuscript. Gisella DePiazza, Nolan Ferguson, Ava Johnson, Andrew Hong, and Olivia Van Der Vlugt helped rear caterpillars.

We acknowledge support from the National Science Foundation's Integrative Research in Biology (IntBIO) Program within the Division of Molecular and Cellular Biosciences (MCB - 2217159) to AYK and WLS. LEE, RKL, and WLS acknowledge support from the Dr. and Mrs. Frederick C. Edie Term Professorship at the University of Florida and from the National Institutes of Health National Institute of General Medical Sciences Maximizing Investigators' Research Award (NIH NIGMS R35-GM147041). Any opinions, findings, and conclusions or recommendations expressed in this manuscript are those of the authors and do not necessarily reflect the views of the National Science Foundation or the National Institutes of Health.

View Article Online
DOI: 10.1039/D5TB01008J

7. Conflict of Interest

The authors declare no competing financial interest.

8. References

1. Holland C, Numata K, Rnjak-Kovacina J, Seib FP. The Biomedical Use of Silk: Past, Present, Future. Adv Healthc Mater. 2019;8(1):e1800465. Epub 20180920. doi: 10.1002/adhm.201800465. PubMed PMID: 30238637.

2. Devi R, Deori M, Devi D. Evaluation of antioxidant activities of silk protein sericin secreted by silkworm Antheraea assamensis (Lepidoptera: Saturniidae). J Pharm Res. 2011;4(12):4688-91.

3. Dong Z, Song Q, Zhang Y, Chen S, Zhang X, Zhao P, Xia Q. Structure, evolution, and expression of antimicrobial silk proteins, seroins in Lepidoptera. Insect Biochem Mol Biol. 2016;75:24-31. Epub 20160513. doi: 10.1016/j.ibmb.2016.05.005. PubMed PMID: 27180727.

4. Manesa KC, Kebede TG, Dube S, Nindi MM. Profiling of Silk Sericin from Cocoons of Three Southern African Wild Silk Moths with a Focus on Their Antimicrobial and Antioxidant Properties. Materials (Basel). 2020;13(24):5706. Epub 20201214. doi: 10.3390/ma13245706. PubMed PMID: 33327575; PMCID: PMC7765042.

5. Aikman EL, Eccles LE, Stoppel WL. Native Silk Fibers: Protein Sequence and Structure Influences on Thermal and Mechanical Properties. Biomacromolecules. 2025;26(4):2043-59. Epub 20250307. doi: 10.1021/acs.biomac.4c01781. PubMed PMID: 40052735; PMCID: PMC12155892.

6. Sehnal F, Sutherland T. Silks produced by insect labial glands. Prion. 2008;2(4):145-53. Epub 20081020. doi: 10.4161/pri.2.4.7489. PubMed PMID: 19221523; PMCID: PMC2658764.

7. Dong Z, Zhao P, Wang C, Zhang Y, Chen J, Wang X, Lin Y, Xia Q. Comparative proteomics reveal diverse functions and dynamic changes of Bombyx mori silk proteins spun from different development stages. J Proteome Res. 2013;12(11):5213-22. Epub 20131008. doi: 10.1021/pr4005772. PubMed PMID: 24093152.

8. Malay AD, Sato R, Yazawa K, Watanabe H, Ifuku N, Masunaga H, Hikima T, Guan J, Mandal BB, Damrongsakkul S, Numata K. Relationships between physical properties and sequence in silkworm silks. Sci Rep. 2016;6:27573. Epub 20160609. doi: 10.1038/srep27573. PubMed PMID: 27279149; PMCID: PMC4899792.

9. Peng Z, Yang X, Liu C, Dong Z, Wang F, Wang X, Hu W, Zhang X, Zhao P, Xia Q. Structural and Mechanical Properties of Silk from Different Instars of Bombyx mori. Biomacromolecules. 2019;20(3):1203-16. Epub 20190213. doi: 10.1021/acs.biomac.8b01576. PubMed PMID: 30702870.

10. Hotaling S, Sproul JS, Heckenhauer J, Powell A, Larracuente AM, Pauls SU, Kelley JL, Frandsen PB. Long Reads Are Revolutionizing 20 Years of Insect Genome Sequencing. Genome Biol Evol. 2021;13(8). doi: 10.1093/gbe/evab138. PubMed PMID: 34152413; PMCID: PMC8358217.

11. Espinosa E, Bautista R, Larrosa R, Plata O. Advancements in long-read genome sequencing technologies and algorithms. Genomics. 2024;116(3):110842. Epub 20240411. doi: 10.1016/j.ygeno.2024.110842. PubMed PMID: 38608738.

View Article Online
DOI: 10.1039/D5TB01008J

12. Childers AK, Geib SM, Sim SB, Poelchau MF, Coates BS, Simmonds TJ, Scully ED, Smith TPL, Childers CP, Corpuz RL, Hackett K, Scheffler B. The USDA-ARS Ag100Pest Initiative: High-Quality Genome Assemblies for Agricultural Pest Arthropod Research. Insects. 2021;12(7):626. Epub 20210709. doi: 10.3390/insects12070626. PubMed PMID: 34357286; PMCID: PMC8307976.

13. Consortium TDToLP, Blaxter M, Mieszkowska N, Di Palma F, Holland P, Durbin R, Richards T, Berriman M, Kersey P, Hollingsworth P, Wilson W, Twyford A, Gaya E, Lawniczak M, Lewis O, Broad G, Howe K, Hart M, Flicek P, Barnes I. Sequence locally, think globally: The Darwin Tree of Life Project. Proceedings of the National Academy of Sciences. 2022;119(4):e2115642118. doi: doi:10.1073/pnas.2115642118.

14. Kawahara AY, Storer CG, Markee A, Heckenhauer J, Powell A, Plotkin D, Hotaling S, Cleland TP, Dikow RB, Dikow T, Kuranishi RB, Messcher R, Pauls SU, Stewart RJ, Tojo K, Frandsen PB. Long-read HiFi sequencing correctly assembles repetitive heavy fibroin silk genes in new moth and caddisfly genomes. GigaByte. 2022;2022:gigabyte64. Epub 20220630. doi: 10.46471/gigabyte.64. PubMed PMID: 36824508; PMCID: PMC9693786.

15. Kmet P, Kucerova L, Sehadova H, Chia-Hsiang Wu B, Wu YL, Zurovec M. Identification of silk components in the bombycoid moth Andraca theae (Endromidae) reveals three fibroin subunits resembling those of Bombycidae and Sphingidae. J Insect Physiol. 2023;147:104523. Epub 20230513. doi: 10.1016/j.jinsphys.2023.104523. PubMed PMID: 37187341.

16. Wu BC, Sauman I, Maaroufi HO, Zaloudikova A, Zurovcova M, Kludkiewicz B, Hradilova M, Zurovec M. Characterization of silk genes in Ephestia kuehniella and Galleria mellonella revealed duplication of sericin genes and highly divergent sequences encoding fibroin heavy chains. Front Mol Biosci. 2022;9:1023381. Epub 20221129. doi: 10.3389/fmolb.2022.1023381. PubMed PMID: 36523651; PMCID: PMC9745057.

17. Kucerova L, Zurovec M, Kludkiewicz B, Hradilova M, Strnad H, Sehnal F. Modular structure, sequence diversification and appropriate nomenclature of seroins produced in the silk glands of Lepidoptera. Sci Rep. 2019;9(1):3797. Epub 20190307. doi: 10.1038/s41598-019-40401-3. PubMed PMID: 30846749; PMCID: PMC6405961.

18. Kono N, Nakamura H, Tateishi A, Numata K, Arakawa K. The balance of crystalline and amorphous regions in the fibroin structure underpins the tensile strength of bagworm silk. Zoological Lett. 2021;7(1):11. Epub 20210726. doi: 10.1186/s40851-021-00179-7. PubMed PMID: 34311769; PMCID: PMC8314566.

19. Shirk BD, Torres Pereira Meriade Duarte I, McTyer JB, Eccles LE, Lateef AH, Shirk PD, Stoppel WL. Harvesting Silk Fibers from Plodia interpunctella: Role of Environmental Rearing Conditions in Fiber Production and Properties. ACS Biomater Sci Eng. 2024;10(4):2088-99. Epub 20240301. doi: 10.1021/acsbiomaterials.3c01372. PubMed PMID: 38427786; PMCID: PMC12074811.

20. Offord C, Vollrath F, Holland C. Environmental effects on the construction and physical properties of Bombyx mori cocoons. Journal of Materials Science. 2016;51(24):10863-72. doi: 10.1007/s10853-016-0298-5. PubMed PMID: WOS:000385410400014.

21. Su H, Cheng Y, Wang Z, Li Z, Stanley D, Yang Y. Silk Gland Gene Expression during Larval-Pupal Transition in the Cotton Leaf Roller Sylepta derogata (Lepidoptera: Pyralidae). PLoS One. 2015;10(9):e0136868. Epub 20150909. doi: 10.1371/journal.pone.0136868. PubMed PMID: 26352931; PMCID: PMC4564283.

View Article Online
DOI: 10.1039/D5TB01008J

22. Zurovec M, Kludkiewicz B, Fedic R, Sulitkova J, Mach V, Kucerova L, Sehnal F. Functional conservation and structural diversification of silk sericins in two moth species. Biomacromolecules. 2013;14(6):1859-66. Epub 20130513. doi: 10.1021/bm400249b. PubMed PMID: 23593923.

23. Lindroth RL. Chemical ecology of the luna moth : Effects of host plant on detoxification enzyme activity. Journal of chemical ecology. 1989;15(7):2019-29. doi: 10.1007/BF01207434. PubMed PMID: 24272292.

24. Millar JG, Haynes KF, Dossey AT, McElfresh JS, Allison JD. Sex Attractant Pheromone of the Luna Moth, Actias luna (Linnaeus). Journal of chemical ecology. 2016;42(9):869-76. Epub 20160820. doi: 10.1007/s10886-016-0751-6. PubMed PMID: 27544534.

25. Markee A, Dansby H, Messcher R, Hernandez E, Kawahara AY, Storer CG. Frass in the class: A model for fostering interest in the natural world through insect rearing in the classroom. American Entomologist. 2021;67(3):24-9.

26. Reddy N, Yang YQ. Investigation of the Structure and Properties of Silk Fibers Produced by. Journal of Polymers and the Environment. 2012;20(3):659-64. doi: 10.1007/s10924-012-0482-x. PubMed PMID: WOS:000308819700004.

27. Chen FJ, Porter D, Vollrath F. Morphology and structure of silkworm cocoons. Materials Science & Engineering C-Materials for Biological Applications. 2012;32(4):772-8. doi: 10.1016/j.msec.2012.01.023. PubMed PMID: WOS:000303299300022.

28. Markee A, Godfrey RK, Frandsen PB, Weng YM, Triant DA, Kawahara AY. De Novo Long-Read Genome Assembly and Annotation of the Luna Moth (Actias luna) Fully Resolves Repeat-Rich Silk Genes. Genome Biol Evol. 2024;16(7):evae148. doi: 10.1093/gbe/evae148. PubMed PMID: 38957923; PMCID: PMC11258402.

29. Foquet B, Eccles LE, Markee A, Triant DA, Frandsen P, Stoppel W, Kawahara A. Evolution of highly repetitive silk genes in the Luna moth, Actias luna. bioRxiv. 2025:2025.08. 07.669095.

30. Hazra S, Chowdhury S, Guha R, Naskar D, Pradhan N, Kundu S, Konar A. Antheraea mylitta silk films with natural RGD sequence supports corneal cell proliferation: A promising new biomaterial for corneal regeneration. Investigative Ophthalmology & Visual Science. 2015;56(7):3470-.

31. Darshan GH, Kong D, Gautrot J, Vootla S. Physico-chemical characterization of Antheraea mylitta silk mats for wound healing applications. Sci Rep. 2017;7(1):10344. Epub 20170904. doi: 10.1038/s41598-017-10531-7. PubMed PMID: 28871135; PMCID: PMC5583262.

32. Bhardwaj N, Rajkhowa R, Wang X, Devi D. Milled non-mulberry silk fibroin microparticles as biomaterial for biomedical applications. Int J Biol Macromol. 2015;81:31-40. Epub 20150729. doi: 10.1016/j.ijbiomac.2015.07.049. PubMed PMID: 26226458.

33. Rockwood DN, Preda RC, Yucel T, Wang X, Lovett ML, Kaplan DL. Materials fabrication from Bombyx mori silk fibroin. Nat Protoc. 2011;6(10):1612-31. Epub 20110922. doi: 10.1038/nprot.2011.379. PubMed PMID: 21959241; PMCID: PMC3808976.

34. Chen Y, Yang W, Wang W, Zhang M, Li M. Bombyx mori Silk Fibroin Scaffolds with Antheraea pernyi Silk Fibroin Micro/Nano Fibers for Promoting EA. hy926 Cell Proliferation. Materials

View Article Online
DOI: 10.1039/D5TB01008J

(Basel). 2017;10(10):1153. Epub 20171003. doi: 10.3390/ma10101153. PubMed PMID: 28972553; PMCID: PMC5666959.

35. Babu PJ, Suamte L. Applications of silk-based biomaterials in biomedicine and biotechnology. Engineered Regeneration. 2024;5(1):56-69.

36. Chen F, Porter D, Vollrath F. Structure and physical properties of silkworm cocoons. J R Soc Interface. 2012;9(74):2299-308. Epub 20120502. doi: 10.1098/rsif.2011.0887. PubMed PMID: 22552916; PMCID: PMC3405738.

37. Rougerie R, Cruaud A, Arnal P, Ballesteros-Mejia L, Condamine FL, Decaëns T, Elias M, Gey D, Hebert PD, Kitching IJ. Phylogenomics illuminates the evolutionary history of wild silkmoths in space and time (Lepidoptera: Saturniidae). bioRxiv. 2022:2022.03. 29.486224.

38. Schneider CA, Rasband WS, Eliceiri KW. NIH Image to ImageJ: 25 years of image analysis. Nat Methods. 2012;9(7):671-5. doi: 10.1038/nmeth.2089. PubMed PMID: 22930834; PMCID: PMC5554542.

39. Edgar RC. MUSCLE: multiple sequence alignment with high accuracy and high throughput. Nucleic Acids Res. 2004;32(5):1792-7. Epub 20040319. doi: 10.1093/nar/gkh340. PubMed PMID: 15034147; PMCID: PMC390337.

40. Schneider TD, Stephens RM. Sequence logos: a new way to display consensus sequences. Nucleic Acids Res. 1990;18(20):6097-100. doi: 10.1093/nar/18.20.6097. PubMed PMID: 2172928; PMCID: PMC332411.

41. Sayers EW, Beck J, Bolton EE, Brister JR, Chan J, Connor R, Feldgarden M, Fine AM, Funk K, Hoffman J, Kannan S, Kelly C, Klimke W, Kim S, Lathrop S, Marchler-Bauer A, Murphy TD, O'Sullivan C, Schmieder E, Skripchenko Y, Stine A, Thibaud-Nissen F, Wang JY, Ye J, Zellers E, Schneider VA, Pruitt KD. Database resources of the National Center for Biotechnology Information in 2025. Nucleic Acids Research. 2024;53(D1):D20-D9. doi: 10.1093/nar/gkae979. PubMed PMID: WOS:001352435500001.

42. Rouhova L, Podlahova S, Kmet P, Zurovec M, Sehadova H, Sauman I. A comprehensive gene expression analysis of the unique three-layered cocoon of the cecropia moth, Hyalophora cecropia. Insect Biochem Mol Biol. 2024;171:104152. Epub 20240627. doi: 10.1016/j.ibmb.2024.104152. PubMed PMID: 38944399.

43. Zurovec M, Yonemura N, Kludkiewicz B, Sehnal F, Kodrik D, Vieira LC, Kucerova L, Strnad H, Konik P, Sehadova H. Sericin Composition in the Silk of Antheraea yamamai. Biomacromolecules. 2016;17(5):1776-87. Epub 20160419. doi: 10.1021/acs.biomac.6b00189. PubMed PMID: 27049111.

44. Tsubota T, Yamamoto K, Mita K, Sezutsu H. Gene expression analysis in the larval silk gland of the eri silkworm Samia ricini. Insect Sci. 2016;23(6):791-804. Epub 20151022. doi: 10.1111/1744-7917.12251. PubMed PMID: 26178074.

45. Dong Y, Dai F, Ren Y, Liu H, Chen L, Yang P, Liu Y, Li X, Wang W, Xiang H. Comparative transcriptome analyses on silk glands of six silkmoths imply the genetic basis of silk structure and coloration. BMC Genomics. 2015;16(1):203. Epub 20150317. doi: 10.1186/s12864-015-1420-9. PubMed PMID: 25886738; PMCID: PMC4372302.

View Article Online
DOI: 10.1039/D5TB01008J

46. Frankenfield AM, Ni J, Ahmed M, Hao L. Protein Contaminants Matter: Building Universal Protein Contaminant Libraries for DDA and DIA Proteomics. J Proteome Res. 2022;21(9):2104-13. Epub 20220706. doi: 10.1021/acs.jproteome.2c00145. PubMed PMID: 35793413; PMCID: PMC10040255.

47. Hu X, Kaplan D, Cebe P. Determining beta-sheet crystallinity in fibrous proteins by thermal analysis and infrared spectroscopy. Macromolecules. 2006;39(18):6161-70. doi: 10.1021/ma0610109. PubMed PMID: WOS:000240069300032.

48. Zhang T, Ma S, Zhang Z, Guo Y, Yang D, Lu W. Overview and Evolution of Insect Fibroin Heavy Chain (FibH). Int J Mol Sci. 2024;25(13):7179. Epub 20240629. doi: 10.3390/ijms25137179. PubMed PMID: 39000286; PMCID: PMC11241164.

49. Moreno-Tortolero RO, Luo Y, Parmeggiani F, Skaer N, Walker R, Serpell LC, Holland C, Davis SA. Molecular organization of fibroin heavy chain and mechanism of fibre formation in Bombyx mori. Commun Biol. 2024;7(1):786. Epub 20240629. doi: 10.1038/s42003-024-06474-1. PubMed PMID: 38951579; PMCID: PMC11217467.

50. Frandsen PB, Hotaling S, Powell A, Heckenhauer J, Kawahara AY, Baker RH, Hayashi CY, Rios-Touma B, Holzenthal R, Pauls SU, Stewart RJ. Allelic resolution of insect and spider silk genes reveals hidden genetic diversity. Proc Natl Acad Sci U S A. 2023;120(18):e2221528120. Epub 20230424. doi: 10.1073/pnas.2221528120. PubMed PMID: 37094147; PMCID: PMC10161007.

51. Heckenhauer J, Plotkin D, Martinez JI, Bethin J, Pauls SU, Frandsen PB, Kawahara AY. Genomic resources of aquatic Lepidoptera, Elophila obliteralis and Hyposmocoma kahamanoa, reveal similarities with Trichoptera in amino acid composition of major silk genes. G3 (Bethesda). 2024;14(9):jkae093. doi: 10.1093/g3journal/jkae093. PubMed PMID: 38722626; PMCID: PMC11373647.

52. Heckenhauer J, Stewart RJ, Rios-Touma B, Powell A, Dorji T, Frandsen PB, Pauls SU. Characterization of the primary structure of the major silk gene, h-fibroin, across caddisfly (Trichoptera) suborders. iScience. 2023;26(8):107253. Epub 20230704. doi: 10.1016/j.isci.2023.107253. PubMed PMID: 37529107; PMCID: PMC10387566.

53. Sezutsu H, Yukuhiro K. Dynamic rearrangement within the Antheraea pernyi silk fibroin gene is associated with four types of repetitive units. J Mol Evol. 2000;51(4):329-38. doi: 10.1007/s002390010095. PubMed PMID: 11040284.

54. SEZUTSU H, UCHINO K, KOBAYASHI I, TAMURA T, YUKUHIRO K. Extensive sequence rearrangements and length polymorphism in fibroin genes in the wild silkmoth, Antheraea yamamai (Lepidoptera, Saturniidae). International journal of wild silkmoth & silk. 2010;15:35-50.

55. Sezutsu H, Yukuhiro K. The complete nucleotide sequence of the Eri-silkworm (Samia cynthia ricini) fibroin gene. Journal of Insect Biotechnology and Sericology. 2014;83(3):3_059-3_70.

56. Gupta AK, Mita K, Arunkumar KP, Nagaraju J. Molecular architecture of silk fibroin of Indian golden silkmoth, Antheraea assama. Sci Rep. 2015;5(1):12706. Epub 20150803. doi: 10.1038/srep12706. PubMed PMID: 26235912; PMCID: PMC4522600.

57. Zhou CZ, Confalonieri F, Medina N, Zivanovic Y, Esnault C, Yang T, Jacquet M, Janin J, Duguet M, Perasso R, Li ZG. Fine organization of Bombyx mori fibroin heavy chain gene. Nucleic Acids

View Article Online
DOI: 10.1039/D5TB01008J

Res. 2000;28(12):2413-9. doi: 10.1093/nar/28.12.2413. PubMed PMID: 10871375; PMCID: PMC102737.

58. Zhou CZ, Confalonieri F, Jacquet M, Perasso R, Li ZG, Janin J. Silk fibroin: structural implications of a remarkable amino acid sequence. Proteins. 2001;44(2):119-22. Epub 2001/06/08. doi: 10.1002/prot.1078. PubMed PMID: 11391774.

59. Kono N, Nakamura H, Ohtoshi R, Tomita M, Numata K, Arakawa K. The bagworm genome reveals a unique fibroin gene that provides high tensile strength. Commun Biol. 2019;2(1):148. Epub 20190429. doi: 10.1038/s42003-019-0412-8. PubMed PMID: 31044173; PMCID: PMC6488591.

60. Yoshioka T, Tsubota T, Tashiro K, Jouraku A, Kameda T. A study of the extraordinarily strong and tough silk produced by bagworms. Nat Commun. 2019;10(1):1469. Epub 20190401. doi: 10.1038/s41467-019-09350-3. PubMed PMID: 30931923; PMCID: PMC6443776.

61. Arakawa K, Kono N, Malay AD, Tateishi A, Ifuku N, Masunaga H, Sato R, Tsuchiya K, Ohtoshi R, Pedrazzoli D, Shinohara A, Ito Y, Nakamura H, Tanikawa A, Suzuki Y, Ichikawa T, Fujita S, Fujiwara M, Tomita M, Blamires SJ, Chuah JA, Craig H, Foong CP, Greco G, Guan J, Holland C, Kaplan DL, Sudesh K, Mandal BB, Norma-Rashid Y, Oktaviani NA, Preda RC, Pugno NM, Rajkhowa R, Wang X, Yazawa K, Zheng Z, Numata K. 1000 spider silkomes: Linking sequences to silk physical properties. Sci Adv. 2022;8(41):eabo6043. Epub 20221012. doi: 10.1126/sciadv.abo6043. PubMed PMID: 36223455; PMCID: PMC9555773.

62. Hayashi CY, Shipley NH, Lewis RV. Hypotheses that correlate the sequence, structure, and mechanical properties of spider silk proteins. Int J Biol Macromol. 1999;24(2-3):271-5. Epub 1999/05/26. doi: 10.1016/s0141-8130(98)00089-0. PubMed PMID: 10342774.

63. Gatesy J, Hayashi C, Motriuk D, Woods J, Lewis R. Extreme diversity, conservation, and convergence of spider silk fibroin sequences. Science. 2001;291(5513):2603-5. doi: 10.1126/science.1057561. PubMed PMID: 11283372.

64. Holland C, Porter D, Vollrath F. Comparing the rheology of mulberry and "wild" silkworm spinning dopes. Biopolymers. 2012;97(6):362-7. Epub 20111209. doi: 10.1002/bip.22011. PubMed PMID: 22161905.

65. Wu N, Zhang S, Li X, Cao Y, Liu X, Wang Q, Liu Q, Liu H, Hu X, Zhou XJ, James AA, Zhang Z, Huang Y, Zhan S. Fall webworm genomes yield insights into rapid adaptation of invasive species. Nat Ecol Evol. 2019;3(1):105-15. Epub 20181210. doi: 10.1038/s41559-018-0746-5. PubMed PMID: 30532047.

66. Takasu Y, Yamada H, Tamura T, Sezutsu H, Mita K, Tsubouchi K. Identification and characterization of a novel sericin gene expressed in the anterior middle silk gland of the silkworm Bombyx mori. Insect Biochem Mol Biol. 2007;37(11):1234-40. Epub 20070801. doi: 10.1016/j.ibmb.2007.07.009. PubMed PMID: 17916509.

67. Gamo T, Inokuchi T, Laufer H. Polypeptides of fibroin and sericin secreted from the different sections of the silk gland in Bombyx mori. Insect Biochemistry. 1977;7(3):285-95.

68. Sehnal F, Akai H. Insect Silk Glands - Their Types, Development and Function, and Effects of Environmental-Factors and Morphogenetic Hormones on Them. International Journal of Insect

View Article Online
DOI: 10.1039/D5TB01008J

Morphology & Embryology. 1990;19(2):79-132. doi: Doi 10.1016/0020-7322(90)90022-H. PubMed PMID: WOS:A1990EA79000002.

69. Masuoka Y, Jouraku A, Tsubota T, Ono H, Chiba H, Sezutsu H, Bono H, Yokoi K. Time-course transcriptome data of silk glands in day 0-7 last-instar larvae of Bombyx mori (w1 pnd strain). Sci Data. 2024;11(1):709. Epub 20240628. doi: 10.1038/s41597-024-03560-1. PubMed PMID: 38942767; PMCID: PMC11213855.

70. Dong Z, Zhao P, Zhang Y, Song Q, Zhang X, Guo P, Wang D, Xia Q. Analysis of proteome dynamics inside the silk gland lumen of Bombyx mori. Sci Rep. 2016;6(1):21158. Epub 20160422. doi: 10.1038/srep21158. PubMed PMID: 27102218; PMCID: PMC4840313.

71. Julien E, Coulon-Bublex M, Garel A, Royer C, Chavancy G, Prudhomme JC, Couble P. 2.11 - Silk Gland Development and Regulation of Silk Protein Genes. In: Gilbert LI, editor. Comprehensive Molecular Insect Science. Amsterdam: Elsevier; 2005. p. 369-84.

72. Sourakov A, Markee A, Stanley EL. CT scanning as a promising tool for studying Lepidoptera immatures. News of the Lepidopterists' Society. 2021;63(2):66-7.

73. Taba M, Gogoi H. Structure of the silk gland of Eri silkworm Samia cynthia ricini Boisd. and its secreted proteins. International Journal of Tropical Insect Science. 2022;42(2):1649-63.

74. Goswami A, Devi D. Exploration of the structural architecture of the silk gland of Antheraea assamensis (Lepidoptera: Saturniidae). ESS Open Archive eprints. 2024;183:18354544.

75. Schmidt T, Puchalla N, Schendzielorz M, Kramell AE. Degumming and characterization of Bombyx mori and non-mulberry silks from Saturniidae silkworms. Sci Rep. 2023;13(1):19504. Epub 20231109. doi: 10.1038/s41598-023-46474-5. PubMed PMID: 37945634; PMCID: PMC10636165.

76. Ferrandin-Schoffel N, Cersoy S, Desrosiers S, Vallard A. Exploring the influence of wild silks composition on dyeing with turmeric and indigo: Spectroscopic insights. Spectrochimica Acta Part A: Molecular and Biomolecular Spectroscopy. 2025;336:126019.

77. Zhang J, Rajkhowa R, Li JL, Liu XY, Wang XG. Silkworm cocoon as natural material and structure for thermal insulation. Materials & Design. 2013;49:842-9. doi: 10.1016/j.matdes.2013.02.006. PubMed PMID: WOS:000318547000102.

78. Eccles LE, Aikman EL, McTyer JB, Cruz ILM, Richgels AL, Stoppel WL. Exploring the functional properties of Plodia interpunctella silk fibers as a natural biopolymer for biomaterial applications. Mater Today Commun. 2025;42. Epub 20241224. doi: 10.1016/j.mtcomm.2024.111416. PubMed PMID: 40636455; PMCID: PMC12237431.

79. Mazzi S, Zulker E, Buchicchio J, Anderson B, Hu X. Comparative thermal analysis of Eri, Mori, Muga, and Tussar silk cocoons and fibroin fibers. J Therm Anal Calorim. 2014;116(3):1337-43. doi: 10.1007/s10973-013-3631-0. PubMed PMID: WOS:000336283600031.

80. Ho M-p, Wang H, Lau K-t, Lee J-h, Hui D. Interfacial bonding and degumming effects on silk fibre/polymer biocomposites. Composites Part B: Engineering. 2012;43(7):2801-12. doi: 10.1016/j.compositesb.2012.04.042.

View Article Online
DOI: 10.1039/D5TB01008J

81. Greco G, Schmuck B, Jalali SK, Pugno NM, Rising A. Influence of experimental methods on the mechanical properties of silk fibers: A systematic literature review and future road map. Biophys Rev (Melville). 2023;4(3):031301. Epub 20230717. doi: 10.1063/5.0155552. PubMed PMID: 38510706; PMCID: PMC10903380.

82. Dyar HG. The number of molts of lepidopterous larvae. Psyche: A Journal of Entomology. 1890;5(175-176):420-2.

83. Inoue S, Tanaka K, Arisaka F, Kimura S, Ohtomo K, Mizuno S. Silk fibroin of Bombyx mori is secreted, assembling a high molecular mass elementary unit consisting of H-chain, L-chain, and P25, with a 6:6:1 molar ratio. J Biol Chem. 2000;275(51):40517-28. Epub 2000/09/15. doi: 10.1074/jbc.M006897200. PubMed PMID: 10986287.

84. Guo K, Zhang X, Zhao D, Qin L, Jiang W, Hu W, Liu X, Xia Q, Dong Z, Zhao P. Identification and characterization of sericin5 reveals non-cocoon silk sericin components with high beta-sheet content and adhesive strength. Acta Biomater. 2022;150:96-110. Epub 20220725. doi: 10.1016/j.actbio.2022.07.021. PubMed PMID: 35902035.

View Article Online
DOI: 10.1039/D5TB01008J

Data Availability Statement:

The data supporting this article have been included as part of the Supplementary Information, where CT measurements of segmented silk glands (Figure S1), amino acid nomenclature (Table S1), degummed silk fiber imaging (Figure S2), FTIR spectra (Figure S3), insect and fiber growth across life stages (Figure S4) can be found.

Raw data can be accessed here:

https://www.dropbox.com/scl/fo/7xi7izwnqrlh9sjlnzbmz/AE2gssml52ZUfinCoS3OUwc?rlkey=d4exe5vv1ynjopzl9jin1epjt&st=33be3d04&dl=0

Article information:

Structure and mechanics of *Actias luna* silk fibers reflect evolutionary and developmental shifts in composition

Lauren E. Eccles,[1] Bert Foquet,[2] Amanda Markee,[2,3] Rebecca K. Liwang,[4] Akito Y. Kawahara,[2] Whitney L. Stoppel[1*]

[1]Department of Chemical Engineering, University of Florida, Gainesville, FL 32611, USA
[2]McGuire Center for Lepidoptera and Biodiversity, Florida Museum of Natural History, University of Florida, Gainesville, FL 32611, USA
[3]American Museum of Natural History, New York, NY 10024, USA
[4]Department of Biology, University of Florida, Gainesville, FL 32611, USA

*Correspondence:

Whitney L. Stoppel, PhD

1006 Center Drive

PO Box 116005

Gainesville, FL 32611

Whitney.stoppel@ufl.edu